



Topological aspects of photonic time crystals

ERAN LUSTIG,[†] YONATAN SHARABI,[†] AND MORDECHAI SEGEV^{*}

Physics Department and Solid State Institute, Technion, 32000 Haifa, Israel

^{*}Corresponding author: msegev@technion.ac.il

Received 10 July 2018; revised 1 October 2018; accepted 3 October 2018 (Doc. ID 338272); published 29 October 2018

We find topological band structures in photonic time crystals—materials in which the refractive index varies periodically and abruptly in time. When the refractive index changes abruptly, the light experiences time refraction and time reflection, analogous to refraction and reflection in photonic crystals. The interference between time-refracted and time-reflected waves gives rise to dispersion bands, which are gapped in the momentum. We show theoretically that photonic time crystals can be in a topologically nontrivial phase, and calculate the topological invariant associated with the momentum bands, which is expressed in the phase between the forward- and backward-propagating waves. When an interface is generated between two time crystals of different topologies, the Zak phase yields a localized interface state, manifested as a localized temporal peak.

© 2018 Optical Society of America under the terms of the OSA

Open Access Publishing Agreement

<https://doi.org/10.1364/OPTICA.5.001390>

1. INTRODUCTION

The past decade has seen rapid development of topological phases of matter in many areas of physics. These phases classify the structure of electronic bands of materials [1] and are robust to the presence of disorder or defects. The study of topological phases led to the discovery of new and exciting materials such as topological insulators [2]. However, topological phases are not only a class of electronic condensed matter systems. Rather, they are a universal wave phenomenon that manifests itself in optics [3], cold-atoms [4,5], acoustics [6,7], exciton–polaritons [8,9], and more. Specifically, in optics, nontrivial topological phases were demonstrated to produce topological edge states [10], robust unidirectional light propagation [11–13], unidirectional lasing [14], highly efficient single mode lasing [15,16], and other exotic phenomena [17,18]. An important class of topological phases in photonics and other fields constitutes one-dimensional (1D) topological systems. In fact, topological phases in photonics were first demonstrated in 1D systems [10] and led to the demonstration of Thouless pumping [19], parity-time symmetric topological systems [20], and more.

An interesting type of crystal that was not related thus far to topological phases is the photonic time crystal (PTC) [21–25]. PTCs are temporal analogues of photonic crystals. While photonic crystals are dielectric materials designed with a refractive index $n(r)$ that varies periodically in space, one can think of a PTC as a dielectric material in which the refractive index changes periodically in time: $n(t)$. For our purposes, the variation in $n(t)$ is externally induced and not an emergent phenomenon. A sudden temporal change in the permittivity ϵ causes time reflections similar to a sudden change of ϵ in space, causing spatial reflections [26–28]. For PTCs, the change in the refractive index should be fast—on the time scale of a few temporal periods of the light or shorter;

otherwise, if the change is not abrupt, a gap might still open, but it will be vanishingly small. Time reflections that occur in a periodic manner lead to interference between forward-propagating waves and time-reversed waves, giving rise to Floquet–Bloch states and dispersion bands, which are gapped in the momentum k , rather than in frequency [23,24]. However, thus far, PTCs were never found to exhibit any relation to topological phases.

Generally, temporal modulation of the refractive index is extremely useful for many purposes such as realizing optical isolators without the magnetic fields, stopping light, and creating synthetic gauge fields for light [29–32]. Importantly, for observing these phenomena, even relatively small changes in the refractive index suffice, as was demonstrated for silicon photonics [33,34]. Small changes in the refractive index cause small bandgaps in momentum, and therefore, in most of these cases, the momentum gaps are not substantial. However, to observe the pronounced features of a PTC, the modulation frequency must be high enough and the amplitude large enough, such that the momentum gaps are substantial and have the same order of magnitude as the momentum of the light propagating in the PTC (otherwise, for small momentum gaps, the observed effects are inconsequential). Thus far, PTCs were demonstrated only at radio frequencies in electronic transmission lines [35]. However, the transition to optical frequencies is close, as PTCs are now attracting growing attention due to recent advances in fabricating dynamic optical systems and metamaterials, and are expected to be observed in the near future [36–38]. In fact, systems with permittivity that varies on short time scales—on the order of the light's temporal period—were demonstrated in many optical systems. Nonlinear effects such as the Kerr nonlinearity in epsilon-near-zero materials [38] and plasma generation [39] can temporarily change the permittivity and refractive index of a material on

very short time scales and at large amplitudes—order of 1. Specifically, the promising results in [38] show that time-modulated materials with large modulation amplitudes in the refractive index are now within fabrication capabilities of modern technology, and that epsilon-near-zero materials are good candidates to create a PTC in the very near future.

Here, we introduce for the first time, to the best of our knowledge, topological phases in PTCs. We describe PTCs displaying a nontrivial topology, which form by periodically modulating the refractive index of a homogenous dielectric medium. We show that PTCs have a topology akin to that of topological insulators. We prove analytically and demonstrate in finite difference time domain (FDTD) simulations, that the topological invariant of the dispersion bands in momentum is related to the relative phase between the forward- and backward-propagating waves generated by the PTC. The topology also gives rise to “temporal topological edge states,” which are the temporal analogue of topological edge states. A temporal edge state is manifested by a localized peak in the amplitude around the time of the temporal edge state. This peak is formed by the interface between two different PTCs, with exponentially decaying tails in both temporal directions.

2. RESULTS

The system we analyze first is a spatially homogeneous material with permittivity $\epsilon(t)$, which is modulated in time, such that $\epsilon(t)$ changes periodically, with period T , in a step-like manner. This results in a binary PTC with two time segments. In the first time segment, $\epsilon(t) = \epsilon_1$ for a duration of t_1 seconds, followed by a second time segment in which $\epsilon(t) = \epsilon_2$ for $t_2 = T - t_1$ seconds [Fig. 1(a)]. For simplicity, the field is polarized in the x direction and propagates in the z direction. This model was studied in [23,24], which showed that this system yields a PTC. Here, we address the topological features of this system and analyze its implications in photonics and topological physics. With every modulation of $\epsilon(t)$, a time reflection occurs, causing waves to partially reflect to their time-reversed pair, while preserving the momentum k due to the homogeneity of space. The time-reversed partner of a wave is a wave with the same momentum but with opposite temporal frequency. This is analogous to a wave conserving its energy and scattering backwards in space in a photonic crystal.

To derive the field propagation in the PTC, we start by describing a linearly polarized wave with momentum k incident on the PTC. In each time segment, the frequency is proportional to the momentum: $\omega_\alpha = kc/n_\alpha$, where α is the segment number and is equal to 1 or 2, $n_\alpha = \sqrt{\epsilon_\alpha}$, k is the vacuum wavenumber of the wave, and c is the speed of light in vacuum.

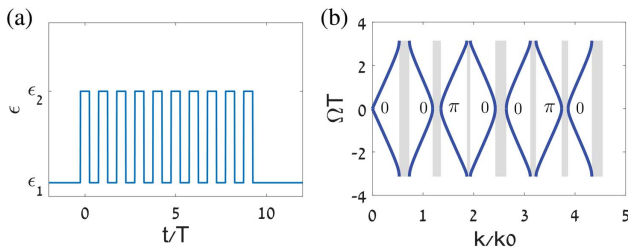


Fig. 1. (a) Binary photonic time crystal (PTC), for $\epsilon_1 = 3$ and $\epsilon_2 = 1$. (b) Dispersion bands of the PTC (blue lines) separated by gaps (gray regions) in momentum (normalized; $k_0 = 2\pi/Tc$). The values (0 and π) labeling each band are the Zak phases associated with the band.

In general, $D(t) = \int_0^\infty f(\tau, t)E(t - \tau)d\tau$, where $D(t)$ is the electric displacement field, and $f(\tau, t)$ is the response function of the material [40], which in our case changes also in time. For simplicity of the analysis, we use an approximation of instantaneous response, meaning that $f(\tau, t) = \epsilon(t)\delta(\tau)$ as in [23]. This simple model of instantaneous response provides the basic physical effects of topological PTCs, which can then be extended to a more realistic non-instantaneous response.

For a periodically modulated instantaneous $\epsilon(t)$, the electric displacement field takes the form

$$D_x^{(\alpha, n)} = (a_n^{(\alpha)} e^{i\omega_\alpha(t + \frac{t}{2} - nT)} + b_n^{(\alpha)} e^{-i\omega_\alpha(t + \frac{t}{2} - nT)})e^{-ikz}, \quad (1)$$

where $D_x^{(\alpha, n)}$ is the electric displacement field in time period n and time segment α , and $a_n^{(\alpha)}$, $b_n^{(\alpha)}$ are complex amplitudes (complex numbers) representing the displacement field amplitudes in each time segment.

Notice that we choose $t = 0$ to be in the middle of time segment 1. This will turn out to be convenient, since it preserves time reversal symmetry. In the same fashion, the magnetic field B_y has a similar form (related through the waves' impedance). The electric displacement field D_x and the magnetic field B_y are continuous between different time segments [27]. Imposing this continuity results in the matrix equation

$$\begin{pmatrix} a_n^{(\alpha)} \\ b_n^{(\alpha)} \end{pmatrix} = \begin{pmatrix} W^{(\alpha)} & -Y^{(\alpha)} \\ -Z^{(\alpha)} & X^{(\alpha)} \end{pmatrix}^n \begin{pmatrix} a_0^{(\alpha)} \\ b_0^{(\alpha)} \end{pmatrix}. \quad (2)$$

The explicit form of $W^{(\alpha)}$, $X^{(\alpha)}$, $Y^{(\alpha)}$, $Z^{(\alpha)}$ is given in Supplement 1. We also note that $W^{(1)} + X^{(1)} = W^{(2)} + X^{(2)} \equiv W + X$. Next, we turn to find the band structure, and the eigenstates of a PTC that is infinite in time. According to the Floquet theorem for each momentum component k , the displacement field assumes the form $D_x = D_\Omega(t)e^{-i\Omega t}e^{ikz}$, where $D_\Omega(t) = D_\Omega(t + T)$. Imposing the Floquet form on Eq. (2) yields the Floquet dispersion relation

$$\Omega(k) = \frac{1}{T} \cos^{-1}(W + X) \quad (3)$$

and the Floquet states

$$\begin{pmatrix} a_n^{(1)} \\ b_n^{(1)} \end{pmatrix} = e^{-i\Omega n T} \begin{pmatrix} Y^{(1)} \\ e^{i\Omega T} - X^{(1)} \end{pmatrix}, \quad (4)$$

where $a_n^{(2)}$ and $b_n^{(2)}$ are obtained by imposing the continuity conditions on $a_n^{(1)}$ and $b_n^{(1)}$. We plot the Floquet frequency Ω as a function of the momentum k in Fig. 1(b), which constitutes the band structure of the PTC. The values of k for which Ω is real are the bands [blue lines in Fig. 1(b)], and the bandgaps are the regions in which Ω is complex [gray regions in Fig. 1(b)].

In many 1D systems, the topological invariant is given by the Zak phase [41]. By analogy, one can formulate the Zak phase of each PTC band as

$$\theta_m^{Zak} = \int_{-\frac{\pi}{T}}^{\frac{\pi}{T}} d\Omega \left[i \int_0^T dt \epsilon(t) D_{m, \Omega}^*(t) \partial_\Omega D_{m, \Omega}(t) \right], \quad (5)$$

where m is the band index, $D_{m, \Omega}(t)$ is the Floquet mode of the displacement field, and θ_m^{Zak} is the Zak phase. We find that the Zak phase takes the values of zero or π for each band (see Supplement 1 for details). As a concrete example, we calculate the Zak phases of the bands of a PTC with $\epsilon_1 = 3$, $\epsilon_2 = 1$, $t_1 = t_2 = 0.5T$, $T = 2$ [fs], and present them in Fig. 1(b) near the appropriate bands. The values of ϵ_1 and ϵ_2 are not

fundamentally important, but their difference $\epsilon_2 - \epsilon_1$ should be on the order of 1 for the effect to be substantial in short PTCs.

The main question at this point is what features are dictated by the Zak phase for light propagating in the PTC. These features are important, since they are topological and therefore should be robust to defects and disorder. We study these properties analytically and verify them in simulation by numerically solving Maxwell's equations with the FDTD method.

To describe the effect of the topology on the PTC, we first need to describe in more detail the characteristic behavior of light inside and outside a bandgap in momentum. To do so, we simulate the propagation of two different pulses inside the PTC. Both pulses have a full width at half maximum of 45 fs. While the first pulse has a center wavelength of $1.4 \mu\text{m}$ that falls within a band, the other has a center wavelength of $0.93 \mu\text{m}$ that falls within the bandgap. At $t = 0$, the pulse starts propagating in free space ($\epsilon = 1$), and at time $t = 220$ fs, a PTC with the same parameters as before starts. The system is linear; therefore, we can decompose the pulse propagation to the propagation of monochromatic plane waves and study it according to Eqs. (1)–(4).

According to Eqs. (1)–(4), after the PTC starts, each plane-wave component of the pulse couples to two Floquet modes, one propagating in the positive z direction (forward propagating), and the other in the negative z direction (time reversed). Figure 2(a) shows the displacement field amplitude of a pulse for which the momentum components reside in a band of the PTC. Since $\Omega(k)$ is real in the bands, the intensity of the pulse remains constant (on average) during propagation. When the PTC ends at $t_{\text{end}} = 340$ [fs] after $n = 60$ periods, the two Floquet modes split again, each coupling back to a forward and time-reversed plane wave. As a result, four different pulses exist after the time crystal ends.

On the other hand, if the momentum components of the pulse fall within the bandgap, $\Omega(k)$ takes a complex value that results in an exponential increase of energy as time progresses. For example, the amplitude of the pulse in Fig. 2(b) is amplified by 20,000 due to the 60 modulation periods constituting the time crystal. We notice that some pulse broadening also occurs as the pulse becomes spatially and temporally wider due to the dispersion of the PTC. The broadening in Fig. 2(b) is by a factor of 2.5, while in Fig. 2(a), it is negligible.

When the time crystal begins, the pulse becomes localized in space with exponentially increasing amplitude. Once the time

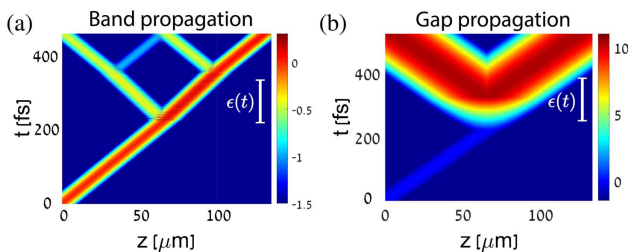


Fig. 2. FDTD simulations, showing the amplitude of the electric displacement field (color bar in log scale) of a pulse propagating under the influence of a PTC. The PTC takes place during the time period marked in white. In (a), the pulse resides in a momentum band, while in (b), it resides in a momentum bandgap. Consequently, the pulse in (a) undergoes two splitting events: when it enters the PTC and when it leaves the PTC, and eventually four pulses emerge from the PTC. On the other hand, in (b), the pulse undergoes a single splitting into two pulses.

crystal ends, the pulse couples to plane waves, but this time the result is two pulses (instead of four for the case of propagation in the band). The two pulses are seen in Fig. 2(b) after the PTC ends. The topological properties of the PTC dictate the phase between these two pulses as we explain next.

It is instructive to compare the effect of the PTC on a pulse to the effect of a spatial photonic crystal. Consider again a 1D spatial photonic crystal—a 1D system of equally spaced layers of alternating refractive indices. When light is incident on this 1D photonic crystal and has frequencies in the bandgap of the spatial photonic crystal, all the light is reflected [Fig. 3(a)]. In this case, the incident wave and the reflected wave have the same amplitude but different phases. The Zak phase dictates the sign of the phase between the incident wave E_i and the reflected wave E_r [42]. In this case, the lattice behaves as a perfect mirror ($E_t = 0$), and the light does not enter the photonic crystal if its frequency falls within a bandgap. Considering now the temporal equivalent, we find that in a PTC, the situation is fundamentally different [Fig. 3(b)]. A wave cannot travel back in time, and therefore all the light enters the PTC, regardless of its momentum—even if it falls within the bandgap. This calls for a new interpretation of the Zak phase for PTCs. It turns out that in a PTC, the Zak phase dictates the sign of the phase between the transmitted wave and the reflected wave, when their momentum is inside the bandgap.

We now describe how the Zak phase dictates the phase difference between the transmitted wave and the reflected wave in a PTC. Consider an incident plane wave $E_i e^{i\omega t}$ experiencing n periods of a PTC [Fig. 1(a)]. The plane wave has wavenumber k inside a bandgap. After the PTC ends, the pulse splits into a time-refracted wave: $A_t E_i e^{i\omega t}$, and a time-reflected wave $A_r E_i e^{-i\omega t}$, as depicted in Fig. 2(b). We find that in this case, asymptotically, $|A_r| = |A_t|$ (assuming n is large enough) [43], but the relative phase $A_r/A_t = e^{i\phi_s}$ is different in each bandgap (marked by s) and for each k . The sign of ϕ_s is determined by the Zak phase according to

$$\text{sgn}(\phi_s) = \delta(-1)^{s+l} \exp\left(i \sum_{m=1}^{s-1} \theta_m^{\text{Zak}}\right), \quad (6)$$

where s is the gap number (lowest gap number is 1), $\delta = \text{sgn}(1 - \frac{\epsilon_1}{\epsilon_2})$, and l is the number of band crossings below gap s . For the first six gaps in our example, $\text{sgn}(\phi_1) = \text{sgn}(\phi_2) = \text{sgn}(\phi_6) = 1$ and $\text{sgn}(\phi_3) = \text{sgn}(\phi_4) = \text{sgn}(\phi_5) = -1$. To derive Eq. (6), we compare the displacement field D_x divided by the magnetic field B_y at t_{end}^+ with the same quantity at time t_{end}^- . This gives the relation

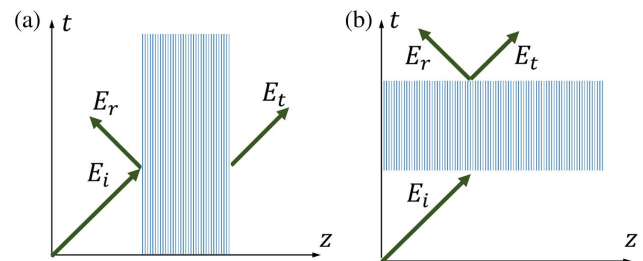


Fig. 3. Reflection and transmission schematics for a monochromatic plane wave incident upon an ordinary 1D photonic crystal—(a), compared to a PTC in (b). In the photonic crystal, if E_i is in a bandgap, E_t is zero, whereas for a PTC, the light always enters the time crystal and passes through it, even if the wavenumber falls within a bandgap.

$$\frac{A_t + A_r}{A_t - A_r} = \frac{n_{\tilde{\alpha}} Y^{(1)} e^{i\omega_{\alpha} t^*} + (e^{i\Omega T} - X^{(1)}) e^{-i\omega_{\alpha} t^*}}{n_{\alpha} Y^{(1)} e^{i\omega_{\alpha} t^*} - (e^{i\Omega T} - X^{(1)}) e^{-i\omega_{\alpha} t^*}}, \quad (7)$$

where $t^* = t_{\text{end}} + t_1/2$, and α is 1 or 2 according to the last segment of the PTC, and $\tilde{\alpha}$ is the index of the PTC segment which is not last. From Eq. (7), the phase between A_t and A_r can be retrieved. The relative phase between two pulses has significant influence on the observables of many systems. For example, coherent control pump–probe experiments and electromagnetically induced transparency depend on this quantity. Furthermore, for short pulses, the relative phase can have an even greater importance as the carrier–envelope phase holds information about the distribution and maximal value of the electric field.

To verify the phase signs obtained analytically from topological considerations (the Zak phase) for the first six gaps, we calculate (numerically) the relative phases between the Floquet modes in the FDTD simulation in Fig. 2(b). We find the phase of each frequency component by Fourier transforming the fields, and then calculating the difference between the frequency component of the time-refracted and time-reversed Floquet modes. The phase differences are plotted in Figs. 4(a)–4(f) for the first six band gaps. The sign of ϕ calculated from our FDTD simulation exactly matches the analytic relation found in Eq. (6) for the entire bandgap. This demonstrates that indeed the relative phase sign between the time-refracted and time-reversed fields in this PTC is determined uniquely by the topological properties of the system.

Topological phases govern the propagation of light in a PTC in additional ways other than the phase just studied. As known from topological physics, when placing two sub-systems with different topological phases next to each other, edge states appear at the interface between them [20,44]. The edge states are eigenstates of the entire system, confined to the region between the two sub-systems. In this context, we ask the following question: what is an edge state in time?

To answer this question, we study the dynamics of light in a system composed of two sequential PTCs, shown in Fig. 5(a). The first PTC has $\epsilon_1 = 3, \epsilon_2 = 1$ and $t_1 = t_2 = 0.5T$, while the second PTC has $\epsilon_2 = 3, \epsilon_1 = 1$ and $t_1 = t_2 = 0.5T$ [Fig. 5(a)]. Thus, the two PTCs have the exact same bandgaps and yet a different topology, manifested in the different Zak phases of their bands. Such two PTCs occur immediately one after the other, as demonstrated in Fig. 5(a), where the interface is a specific time point $t_{\text{edge}} = 8T$. We find that a topological

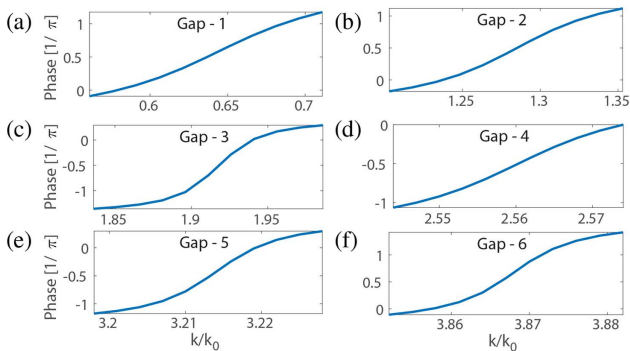


Fig. 4. (a)–(f) Phase difference ϕ between the forward- and backward-propagating Floquet modes of the first six gaps of the PTC, obtained from FDTD simulations. These results match the calculation based on the topological invariant—the Zak phase, in Eqs. (5) and (6).

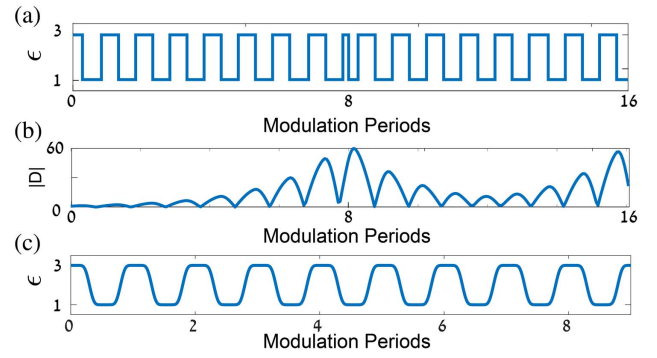


Fig. 5. Temporal topological edge states between two PTCs. (a) Two PTCs with different Zak phases cascaded at $t = 8T$. (b) The amplitude of the displacement field of the pulse propagating in the PTC plotted in (a). The light’s amplitude increases exponentially in time up to the interface between PTCs at $t = 8T$. Immediately after the interface, the amplitude starts to decrease exponentially, before eventually returning to its normal bandgap behavior of an exponential increase as the time progresses. The result is an amplitude peak localized at the time of the interface between PTCs. (c) Time lattice with smooth modulation.

edge state forms at the temporal interface between two PTCs. Such an edge state in time is essentially a temporal exponential increase in amplitude towards t_{edge} followed by a temporal exponential decrease right after. The peak amplitude of this process is at t_{edge} . After the light amplitude decreases, it begins to increase once again. We plot the displacement field’s amplitude of the pulse in the PTC as a function of time near the temporal edge state in Fig. 5(b). The temporal topological edge state is similar in nature to the spatial edge state between two concatenated Su–Schrieffer–Heeger (SSH) lattices [20,42,44].

It is instructive to compare our results on temporal topological edge states between two PTCs and spatial topological edge states between two crystals. In the spatial case, the topological edge states always exhibit exponential decay on both sides of the interface. Topological edge states of PTCs, on the other hand, exist between regions that each support exponential increase of the amplitude. Thus, the phenomenon observed in PTCs of a peak decaying in both temporal directions is completely counterintuitive. This decrease in amplitude on either side of the topological temporal edge state between two PTCs means that the external modulation extracts energy from the system, which can have many implications.

At this point, we wish to examine a more realistic case in which the modulation of the refractive index is not step-like, but smooth [with $\epsilon(t)$ still instantaneous with the polarization]. In this context, the main question arising is whether the topological invariants 0 or π still have physical implications after the smoothening of the step-like modulations previously discussed. In the smooth case, the electromagnetic wave equation for a PTC has a more complicated form and should be solved numerically. Naturally, such smooth modulation is more physical and more general. Thus, in the case of time-dependent $\epsilon(t)$ with instantaneous response, the wave equation for the electric field \mathbf{E} , derived from the Maxwell equations, takes the form

$$\nabla^2 \mathbf{E} = \epsilon(t) \mu \frac{\partial^2 \mathbf{E}}{\partial t^2} + 2\mu \dot{\epsilon}(t) \frac{\partial \mathbf{E}}{\partial t} + \mu \ddot{\epsilon}(t) \mathbf{E}, \quad (8)$$

where μ is a constant magnetic permeability.

We find (numerically) that the eigenmodes of Eq. (8)—with ϵ modulated smoothly in time [Fig. 5(c)]—do conserve the properties dictated by the integer Zak phases of the step-like model, despite the derivative terms added on the right-hand side of Eq. (8) (see Supplement 1). Observing Eq. (8) for a periodic (temporally infinite) smoothly time-modulated $\epsilon(t)$, the equation has time-translation symmetry by the lattice time period T , and thus has Floquet eigenmodes. Moreover, Eq. (8) is symmetric with respect to time inversion $\epsilon(t) = \epsilon(-t)$. Due to those two symmetries, the implications of the Zak phase are not lost by the smoothening [41]. Consequently, a relatively small smoothening as in Fig. 5(c) does not alter the phases of the bandgaps in Fig. 4. In this context, measuring the phase sign numerically between pulses emitted from the smooth PTC in Fig. 5(c) gives the same results as for the step-like PTC in Fig. 1(a) (see Supplement 1).

It is important to clarify that the phase relation and the effects of the Zak phase are not exclusive to pulses, but universal to all electromagnetic plane waves propagating in the linear PTC. The FDTD simulations describe the linear propagation of pulses, which are a superposition of plane waves and therefore describe the dynamics of all the different plane wave frequencies.

Last but not least, we propose a realization for the topological PTC with an epsilon-near-zero material based on Al-doped zinc oxide. Very recently, it was demonstrated that the refractive index of this material can be set to vary uniformly in time from near-zero values to values on the order of 1 at optical frequencies [38,45,46]. As we explained here, observing the temporal topological effects in PTCs requires a material that can change its refractive index amplitude by order of 1 on a few femto-seconds time scale. Thus, the system of [38,45,46] is an excellent candidate for exploring topological effects in PTCs. We also stress that, regardless of its interesting properties, measuring the topological properties of a PTC is also a useful approach for studying PTCs in experiments. The reason is that topological phenomena are fundamentally robust to disorder, and therefore topological lattices produce exact measurements even when fabricated with low accuracy, as is typically the case in pioneering experiments. Furthermore, the topology here is applicable for the entire electromagnetic spectrum; thus, it can also be demonstrated even at radio frequencies in electronic transmission lines [35].

3. CONCLUSION

Before closing, we would like to emphasize the similarities and differences between the topological PTC presented here and another class of topological systems arising from temporal modulation: Floquet topological insulators [47], which were demonstrated in photonics [12]. The topology we present here is fundamentally different from Floquet topological insulators. In Floquet topological insulators, the driving field, which is a temporal modulation, is auxiliary designed for opening a topological gap in the frequency dispersion $\omega(k)$ of a crystal, i.e., of a system that is periodic in space. In contradistinction, for PTCs, the time is the crystalline dimension itself. Hence, the abrupt temporal variations in PTCs open a topological gap in momentum k and not in frequency ω . This is a property of systems governed by equations with a second derivative in time, such as the wave equation in electromagnetism. Consequently, the ideas proposed here are relevant to virtually any wave system in nature, where the properties of the medium can be varied in time.

In conclusion, we studied a topological PTC, proved that it has distinct topological phases, and demonstrated how they affect the propagation of light inside the PTC. Understanding the topological phenomena associated with PTCs can lead to many interesting avenues of research. For example, many interesting topological phenomena appear only in dimensions higher than one. Here, even though there is only one time dimension, adding a PTC to spatial 1D lattices (such as the SSH lattice) would lead to the formation of topological insulators in space–time. Finally, we note that PTCs also have interesting quantum properties [48], as they are related to photon pair production from the vacuum state and to squeezed light [43]. Undoubtedly, experimental avenues for realizing PTCs are now rapidly developing, and experiments with PTCs are expected in the near future. Unraveling the topological aspects of PTCs, along with their classical and quantum properties would greatly help in understanding the fundamental nature of time, light, and periodic phenomena.

Note added in proof: we note a related manuscript on topological time crystals that appeared on the arXiv while our paper was under review [49].

Funding. Israel Excellence Center ICORE Program “Circle of Light,” Israel Science Foundation (ISF); H2020 European Research Council (ERC).

Acknowledgment. E. L. is grateful for the support of the Adams Fellowship by the Israel Academy of Sciences.

See Supplement 1 for supporting content.

[†]These authors contributed equally to this work.

REFERENCES

1. D. Thouless, M. Kohmoto, M. Nightingale, and M. den Nijs, “Quantized Hall conductance in a two-dimensional periodic potential,” *Phys. Rev. Lett.* **49**, 405–408 (1982).
2. C. L. Kane and E. J. Mele, “Topological order and the quantum spin Hall effect,” *Phys. Rev. Lett.* **95**, 146802 (2005).
3. F. D. M. Haldane and S. Raghu, “Possible realization of directional optical waveguides in photonic crystals with broken time-reversal symmetry,” *Phys. Rev. Lett.* **100**, 013904 (2008).
4. M. Atala, M. Aidelsburger, J. T. Barreiro, D. Abanin, T. Kitagawa, E. Demler, and I. Bloch, “Direct measurement of the Zak phase in topological Bloch bands,” *Nat. Phys.* **9**, 795–800 (2013).
5. G. Jotzu, M. Messer, R. Desbuquois, M. Lebrat, T. Uehlinger, D. Greif, and T. Esslinger, “Experimental realization of the topological Haldane model with ultracold fermions,” *Nature* **515**, 237–240 (2014).
6. A. B. Khanikaev, R. Fleury, S. H. Mousavi, and A. Alù, “Topologically robust sound propagation in an angular-momentum-biased graphene-like resonator lattice,” *Nat. Commun.* **6**, 8260 (2015).
7. C. He, X. Ni, H. Ge, X.-C. Sun, Y.-B. Chen, M.-H. Lu, X.-P. Liu, and Y.-F. Chen, “Acoustic topological insulator and robust one-way sound transport,” *Nat. Phys.* **12**, 1124–1129 (2016).
8. P. St-Jean, V. Goblot, E. Galopin, A. Lemaître, T. Ozawa, L. Le Gratiet, I. Sagnes, J. Bloch, and A. Amo, “Lasing in topological edge states of a one-dimensional lattice,” *Nat. Photonics* **11**, 651–656 (2017).
9. S. Klembt, T. H. Harder, O. A. Egorov, K. Winkler, R. Ge, M. A. Bandres, M. Emmerling, L. Worschech, T. C. H. Liew, M. Segev, C. Schneider, and S. Höfling, “Exciton-polariton topological insulator,” *Nature* (2018), doi: 10.1038/s41586-018-0601-5.
10. N. Malkova, I. Hromada, X. Wang, G. Bryant, and Z. Chen, “Observation of optical Shockley-like surface states in photonic superlattices,” *Opt. Lett.* **34**, 1633–1635 (2009).

11. Z. Wang, Y. Chong, J. D. Joannopoulos, and M. Soljačić, "Observation of unidirectional backscattering-immune topological electromagnetic states," *Nature* **461**, 772–775 (2009).
12. M. C. Rechtsman, J. M. Zeuner, Y. Plotnik, Y. Lumer, D. Podolsky, F. Dreisow, S. Nolte, M. Segev, and A. Szameit, "Photonic Floquet topological insulators," *Nature* **496**, 196–200 (2013).
13. M. Hafezi, S. Mittal, J. Fan, A. Migdall, and J. M. Taylor, "Imaging topological edge states in silicon photonics," *Nat. Photonics* **7**, 1001–1005 (2013).
14. B. Bahari, A. Ndao, F. Vallini, A. El Amili, Y. Fainman, and B. Kanté, "Nonreciprocal lasing in topological cavities of arbitrary geometries," *Science* **358**, 636–640 (2017).
15. G. Harari, M. A. Bandres, Y. Lumer, M. C. Rechtsman, Y. D. Chong, M. Khajavikhan, D. N. Christodoulides, and M. Segev, "Topological insulator laser: theory," *Science* **359**, eaar4003 (2018).
16. M. A. Bandres, S. Wittek, G. Harari, M. Parto, J. Ren, M. Segev, D. N. Christodoulides, and M. Khajavikhan, "Topological insulator laser: experiments," *Science* **359**, eaar4005 (2018).
17. J. M. Zeuner, M. C. Rechtsman, Y. Plotnik, Y. Lumer, S. Nolte, M. S. Rudner, M. Segev, and A. Szameit, "Observation of a topological transition in the bulk of a non-Hermitian system," *Phys. Rev. Lett.* **115**, 040402 (2015).
18. O. Zilberberg, S. Huang, J. Guglielmon, M. Wang, K. P. Chen, Y. E. Kraus, and M. C. Rechtsman, "Photonic topological boundary pumping as a probe of 4D quantum Hall physics," *Nature* **553**, 59–62 (2018).
19. Y. E. Kraus, Y. Lahini, Z. Ringel, M. Verbin, and O. Zilberberg, "Topological states and adiabatic pumping in quasicrystals," *Phys. Rev. Lett.* **109**, 106402 (2012).
20. S. Weimann, M. Kremer, Y. Plotnik, Y. Lumer, S. Nolte, K. G. Makris, M. Segev, M. C. Rechtsman, and A. Szameit, "Topologically protected bound states in photonic parity-time-symmetric crystals," *Nat. Mater.* **16**, 433–438 (2017).
21. D. Holberg and K. Kunz, "Parametric properties of fields in a slab of time-varying permittivity," *IEEE Trans. Antennas Propag.* **14**, 183–194 (1966).
22. A. B. Shvartsburg, "Optics of nonstationary media," *Phys. Usp.* **48**, 797–823 (2005).
23. F. Biancalana, A. Amann, A. V. Uskov, and E. P. O'Reilly, "Dynamics of light propagation in spatiotemporal dielectric structures," *Phys. Rev. E* **75**, 046607 (2007).
24. J. R. Zurita-Sánchez, P. Halevi, and J. C. Cervantes-González, "Reflection and transmission of a wave incident on a slab with a time-periodic dielectric function $\epsilon(t)$," *Phys. Rev. A* **79**, 053821 (2009).
25. J. R. Zurita-Sánchez, J. H. Abundis-Patiño, and P. Halevi, "Pulse propagation through a slab with time-periodic dielectric function $\epsilon(t)$," *Opt. Express* **20**, 5586–5600 (2012).
26. F. R. Morgenthaler, "Velocity modulation of electromagnetic waves," *IRE Trans. Microwave Theory Tech.* **6**, 167–172 (1958).
27. J. Mendonca, *Theory of Photon Acceleration* (CRC Press, 2000).
28. V. Bacot, M. Labousse, A. Eddi, M. Fink, and E. Fort, "Time reversal and holography with spacetime transformations," *Nat. Phys.* **12**, 972–977 (2016).
29. M. F. Yanik and S. Fan, "Time reversal of light with linear optics and modulators," *Phys. Rev. Lett.* **93**, 173903 (2004).
30. S. Longhi, "Stopping and time reversal of light in dynamic photonic structures via Bloch oscillations," *Phys. Rev. E* **75**, 026606 (2007).
31. Z. Yu and S. Fan, "Complete optical isolation created by indirect interband photonic transitions," *Nat. Photonics* **3**, 91–94 (2009).
32. K. Fang, Z. Yu, and S. Fan, "Realizing effective magnetic field for photons by controlling the phase of dynamic modulation," *Nat. Photonics* **6**, 782–787 (2012).
33. P. Dong, S. F. Preble, J. T. Robinson, S. Manipatruni, and M. Lipson, "Inducing photonic transitions between discrete modes in a silicon optical microcavity," *Phys. Rev. Lett.* **100**, 033904 (2008).
34. H. Lira, Z. Yu, S. Fan, and M. Lipson, "Electrically driven nonreciprocity induced by interband photonic transition on a silicon chip," *Phys. Rev. Lett.* **109**, 033901 (2012).
35. J. R. Reyes-Ayona and P. Halevi, "Observation of genuine wave vector (k or β) gap in a dynamic transmission line and temporal photonic crystals," *Appl. Phys. Lett.* **107**, 074101 (2015).
36. A. Shaltout, A. Kildishev, and V. Shalaev, "Time-varying metasurfaces and Lorentz non-reciprocity," *Opt. Mater. Express* **5**, 2459–2467 (2015).
37. M. Artamonov and T. Seideman, "Time-dependent, optically controlled dielectric function," *J. Phys. Chem. Lett.* **6**, 320–325 (2015).
38. S. Vezzoli, V. Bruno, C. DeVault, T. Roger, V. M. Shalaev, A. Boltasseva, M. Ferrera, M. Clerici, A. Dubietis, and D. Faccio, "Optical time reversal from time-dependent epsilon-near-zero media," *Phys. Rev. Lett.* **120**, 043902 (2018).
39. E. Yablonovitch, "Accelerating reference frame for electromagnetic waves in a rapidly growing plasma: Unruh-Davies-Fulling-DeWitt radiation and the nonadiabatic Casimir effect," *Phys. Rev. Lett.* **62**, 1742–1745 (1989).
40. L. D. Landau, E. M. Lifshitz, and A. L. King, *Electrodynamics of Continuous Media*, Course of Theoretical Physics (Butterworth, 1961).
41. J. Zak, "Berry's phase for energy bands in solids," *Phys. Rev. Lett.* **62**, 2747–2750 (1989).
42. M. Xiao, Z. Q. Zhang, and C. T. Chan, "Surface impedance and bulk band geometric phases in one-dimensional systems," *Phys. Rev. X* **4**, 021017 (2014).
43. J. T. Mendonça, G. Brodin, and M. Marklund, "Vacuum effects in a vibrating cavity: time refraction, dynamical Casimir effect, and effective Unruh acceleration," *Phys. Lett. A* **372**, 5621–5624 (2008).
44. A. Blanco-Redondo, I. Andonegui, M. J. Collins, G. Harari, Y. Lumer, M. C. Rechtsman, B. J. Eggleton, and M. Segev, "Topological optical waveguiding in silicon and the transition between topological and trivial defect states," *Phys. Rev. Lett.* **116**, 163901 (2016).
45. N. Kinsey, C. DeVault, J. Kim, M. Ferrera, V. M. Shalaev, and A. Boltasseva, "Epsilon-near-zero Al-doped ZnO for ultrafast switching at telecom wavelengths," *Optica* **2**, 616–622 (2015).
46. M. Clerici, N. Kinsey, C. DeVault, J. Kim, E. G. Carnemolla, L. Caspani, A. Shaltout, D. Faccio, V. Shalaev, A. Boltasseva, and M. Ferrera, "Controlling hybrid nonlinearities in transparent conducting oxides via two-colour excitation," *Nat. Commun.* **8**, 15829 (2017).
47. N. H. Lindner, G. Refael, and V. Galitski, "Floquet topological insulator in semiconductor quantum wells," *Nat. Phys.* **7**, 490–495 (2011).
48. M. Artoni, A. Bulatov, and J. Birman, "Zero-point noise in a nonstationary dielectric cavity," *Phys. Rev. A* **53**, 1031–1035 (1996).
49. K. Giergiel, A. Dauphin, M. Lewenstein, J. Zakrzewski, and K. Sacha, "Topological time crystals," arXiv: 1806.10536 (2018).